Microstructure Influence on Rock Electrical Properties: Integration of Laboratory and Numerical Methods

Muhammad Bisri Mustofa 1,*, Aditya Awalludien Wicahyanto1, Firda Mahfuziahaq1, Supriyanto1

¹ Geosciences Department, FMIPA, Universitas Indonesia

*Corresponding author: bisrimustofa.bm@gmail.com

Abstract

The electrical properties of rocks are widely used in characterizing reservoir rocks due to their ability to identify porosity, fluid types, and saturation levels. This study aims to determine the effect of microstructure on the electrical properties of Ngrayong Formation rocks through laboratory measurements and numerical calculations. Twelve samples from three-grain size categories were prepared for resistivity measurements under partially and fully brine-saturated conditions using a 6% NaCl solution. Scanning results of the three categories revealed that grain size influences the microstructure of rocks, including the distribution of grain size and pore size. The estimated electrical properties show that at low saturation, microstructure significantly affects the resistivity response, as indicated by porosity values ranging from 34% to 48%. Conversely, at high saturation, variations in microstructure tend to result in uniform resistivity, indicating minor microstructural influence on high-saturation electrical property estimations. Additionally, Archie parameters were determined with ranges of 2.1-3.4 for the cementation exponent and 1.2-2.4 for the saturation exponent. A strong correlation was also observed between laboratory measurements and numerical calculations for all porosity ranges, especially for samples with small grain sizes for all porosity ranges. This study provides a deeper understanding of the electrical properties of rocks as a function of their microstructure, which can serve as a base for interpreting electrical data from Routine/Special Core Analysis, resistivity log data, or field resistivity data in Applied Geophysics.

Keywords: Electrical Resistivity, Ngrayong Formation, Laboratory Measurements, Numerical Calculation

1. Introduction

Geophysical surveys provide spatial subsurface information without causing damage. One such method uses the electrical properties of rocks to assess geological features and map structures (Zhou & Zhang, 2020). The sensitivity of geological layers to resistivity offers key insights for monitoring subsurface properties (Vozar & Gurevich, 2014). Although rocks are typically poor conductors, the presence of conductive fluids in pore spaces can enhance their conductivity. The relationship between resistivity and fluid saturation in rocks was studied by Archie (1942), who proposed the following empirical formula:

$$\rho = \phi^{-m} S_w^{-n} \rho_w \dots (1.1)$$

where ρ is the resistivity of a partially saturated rock sample, ϕ is the sample porosity, S_w is the fluid saturation, ρ_w is the fluid resistivity, and m and

n are the cementation and saturation exponents, respectively. For fully saturated rocks, the following formula applies:

$$\rho_o = a \, \phi^{-m} \dots (1.2)$$

where ρ_o is the resistivity of the rock sample in fully saturated conditions and a is a constant. Archie (1942) reported that m typically ranges 1.80 to 2.00 for consolidated sands and approximately 1.30 for unconsolidated sands, while n is typically around 2 for both types. These parameters, m and n, are critical for predicting rock porosity and fluid content (Sezgin & Akın, 2013; Glover, 2017). As a result, research on these parameters continues to evolve until nowadays.

Microstructure, including pore structures, influences the values of m and n (Tariq & Kazi, 2017). Torskaya et al. (2014) suggested that variations in grain shape affect porosity by influencing particle arrangement and packing. The

relationship between porosity and resistivity is not always consistent, even within the same rock type, due to variations in mineral composition and pore geometry (Verwer et al., 2011). Additionally, the resistivity of hydrocarbon-saturated rocks is highly sensitive to changes in *m* and *n* (Glover, 2017). To understand how pore structures affect rock resistivity, microscopic-scale observations are required, which are challenging to achieve with conventional methods.

Conventional modeling of rock structures typically relies on empirical relationships derived from idealized microstructural models. However, this approach has significant limitations, including the inability to capture the full range of pore structure variations across different rocks and the lengthy sample preparation process (Mustofa et al., 2022). Additionally, these models fail to represent the diverse microstructures present in natural rocks (Andrä et al., 2013). Microstructural information can be obtained using computed tomography, which employs X-ray radiation to generate digital images of rock pore structures at the microscopic scale. By analyzing these digital images, electrical properties can be estimated. This technique, known as Digital Rock Physics (DRP), is commonly used to analyze the physical properties of rocks (Andrä et al., 2013a; Andrä et al., 2013b).

Image processing methods have advanced significantly in recent decades (Blunt et al., 2013), enabling detailed characterization and visualization of objects. Studies by Latief et al. (2017) and Nabahan et al. (2019) employed Micro-CT scans to quantitatively measure rock structural elements. Unlike destructive geotechnical methods, image processing is non-destructive, preserving samples for future analysis. Micro-CT scanning can achieve resolutions of up to 5 micrometers per pixel (Latief et al., 2017). Digital Rock Physics (DRP) provides insights into how pore structures influence electrical properties, which can then be compared with laboratory measurements.

The Ngrayong Formation is one of Indonesia's significant oil and gas reservoirs with a porosity of around 33%, serving as a major hydrocarbon source in several oil fields within the North East Java Basin (Nababan et al., 2019). Dominated by clean sand lithology, it is a primary reservoir in the Rembang Zone, particularly within the Cepu Block (Dhamayanti et al., 2016). Kadar (1993) described the formation as comprising quartz sandstone with angular to subangular grains. The Ngrayong Formation has been crucial in establishing the Rembang Zone as a key oil and gas-producing basin in Indonesia.

This study investigates the impact of pore structure on the electrical properties of unconsolidated sandstone samples from outcrops of the Ngrayong Formation, a primary oil reservoir in the Cepu Block, East Java. Electrical property analysis was performed by integrating laboratory measurements with Digital Rock Physics (DRP) simulations. The results reveal relationships between physical properties and pore structure, as represented by Archie parameters. This study aims to enhance core sample analysis in oil and gas resource evaluations.

2. Materials and Method

2.1. Sample Description and Preparation

The Ngrayong Formation, dating to the Middle Miocene, consists of quartz sandstone with fine grains at the base, transitioning to coarser grains and occasional calcareous layers at the top (Pringgoprawiro, 1983). Initially classified as a member of the Tawun Formation, it was later reclassified as the Ngrayong Formation. Regionally, it was deposited in a tidal environment with predominantly clean sand lithology (Arbol & Bahar, 2021). In this study, unconsolidated sandstone samples from exposed sections of the Ngrayong Formation were used to investigate the influence of pore structure on electrical properties. Twelve rock samples with varying grain sizes were

selected to ensure a range of microstructures. The samples were placed in cylindrical acrylic holders with diameters of 3.8 cm and heights of 3.6 cm and were prepared with relatively uniform porosities ranging from 35% to 45%. Prior to placement in the holders, all samples were oven-dried for 24 hours at 120°C to ensure complete dryness. The samples

were categorized as either fully saturated (9 samples) or partially saturated (3 samples). Fully saturated samples were used to derive Archie parameters m and n. Brine injections were performed according to the procedures outlined by Mustofa et al. (2021). The characteristics of the twelve samples are summarized in Table 1.

Table 1. Characteristics of the twelve samples categorized into three groups (A, B, and C) with porosity ranges from 34% to 48%.

Rock Sample	Grain size (no. sieve)	Density (gram/cm³)	Condition	Porosity (%)
A2	45,17			
A3	41,19			
A4		38,82		
A5		36,66		
A6	Partially Saturated	40,11		
B1	0,250 – 0,425 mm (40 – 60)	2,69	Fully Saturated	41,24
B2				39,41
В3				37,47
B4				34,66
B5			Partially Saturated	39,84
C1	< 0,250 (< 60)	2,61	Partially Saturated	39,72

2.2. Laboratory Measurement of Electrical Resistivity

Electrical resistivity measurements were conducted using a resistivity meter designed with electronic components for current injection and for measuring voltage, current, and resistance. The entire measurement process was controlled using an STM32 Learning Board, an ARM Cortex-M4

microcontroller. The measurements began by placing rock samples into acrylic sample holders with an inner diameter of 3.8 cm and a height of 3.6 cm. The resistivity meter was connected to the sample holder using two copper electrodes: potential electrodes (P+ and P-) and current electrodes (C+ and C-). The setup of the resistivity meter is illustrated in Figure 1.

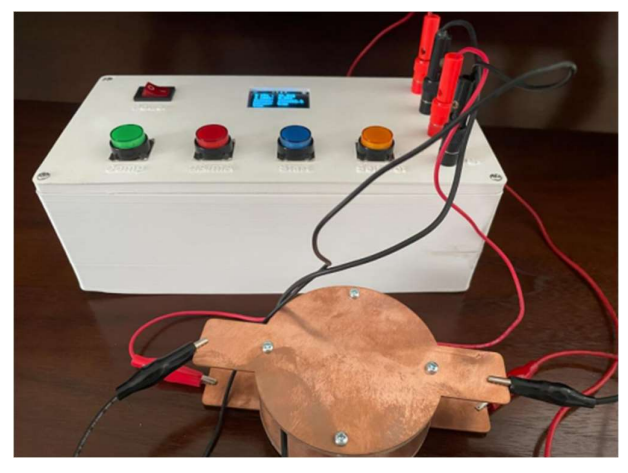


Figure 1. Well-calibrated resistivity meter used to analyze the physical properties of rock samples.

Measurements were conducted under two conditions: fully saturated and partially saturated. The fully saturated condition was used to examine the relationship between resistivity and porosity, while the partially saturated condition focused on the relationship between resistivity and water saturation. A brine solution with a 6% NaCl concentration was used as the saturating fluid. For partially saturated samples (A6, B5, and C1), brine was incrementally injected into the center of the sample holder, with saturation levels ranging from 10% to 100%. For the remaining samples, brine was directly injected to achieve full saturation. The resulting resistivity data were processed to produce graphs showing resistivity as a function of saturation and porosity.

2.3. Calculation of Electrical Resistivity

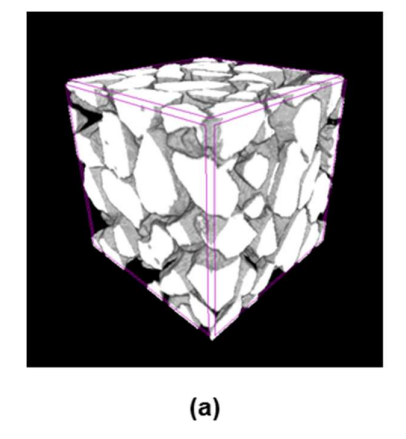
Numerical calculations of electrical resistivity using Digital Rock Physics (DRP) involved three main stages: digital image acquisition, image processing, and physical property computation (Andrä et al., 2013).

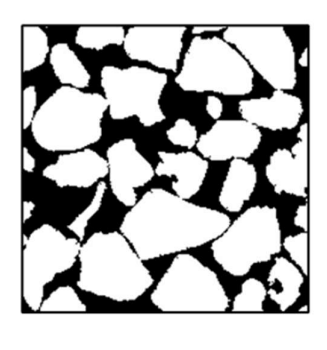
Image Acquisition: Samples were scanned in their dry state using a SkyScan 1173 X-ray micro-

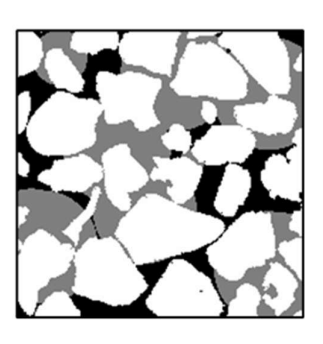
CT scanner (Bruker MicroCT, Kontich, Belgium) with high-resolution settings. The scanner operated at 55 kV and 90 μ A, with an X-ray transmission range of 30%-90% (Mustofa et al., 2022). The resulting scans were reconstructed into 8-bit grayscale images.

Image Processing: Segmentation was performed to distinguish matrix and air phases using manual thresholding based on the X-ray absorption histogram. Fluid phases were modeled following prior studies, with saturation levels varying from 10% to 100% (Mustofa et al., 2022). The processed images are presented in Figure 2.

Electrical Resistivity Calculation: Resistivity calculations were conducted using the open-source code ELECFEM3D.f, developed by the National Institute of Standards and Technology (NISTIR) (Garboczi, 1998). The finite element method (FEM) was applied to divide the sample into small elements and calculate global bulk resistivity. Initial resistivity inputs were assigned for each phase: matrix (∞), air (0.001 Ω ·m), and brine (0.1033 Ω ·m). The simulation results were compared with laboratory measurements to enhance understanding of rock pore structures.







(b)

Figure 2. (a) 3D reconstructed image of rock samples. (b) 2D image showing black (pores), white (rock grains), and gray (fluid saturation in pore spaces).

3. Results and Discussion

3.1 Rock Sample Resistivity vs Porosity

Electrical resistivity measurements as a function of porosity were conducted under two

conditions: dry and fully saturated. For samples A and B, with porosity ranges of 34%-49%, measurements under dry conditions showed that resistivity increased with higher porosity, as

illustrated in Figure 3. Resistivity values ranged from $1.2 \times 10^5 - 1.8 \times 10^5$ ohm.m. This trend arises because the absence of conductive media (e.g., fluids) in the pore spaces inhibits electrical conduction. Larger pore spaces result in higher bulk resistivity for both sample categories. The resistivity-porosity relationship under dry conditions can be expressed as $y = 297x^{1.0433}$ with $R^2 = 0.8048$.

Under fully saturated conditions, resistivity decreased logarithmically with increasing porosity, consistent with Archie's Law (Equation 1.2). The cementation exponent (*m*) was determined to be 3,418. While this value is slightly higher than the range reported by Archie (1942), it aligns with the findings of Verwer et al. (2011). This trend was observed for both sample categories, suggesting that at full saturation, grain size has minimal influence on bulk resistivity.

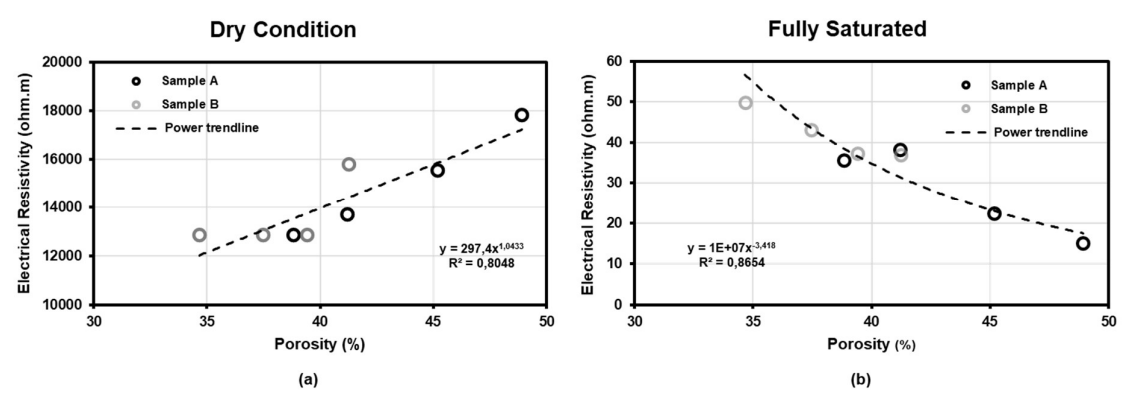


Figure 3. Relationship between measured resistivity and porosity for (a) dry conditions and (b) fully saturated conditions.

3.2 Rock Sample Resistivity vs Saturation

Measurements under partially saturated conditions are shown in Figure 4. The results indicate that resistivity decreases as fluid saturation increases. From 0% to 40% saturation, resistivity exhibits a sharp decline, as reflected by the steep slope of the graph. Beyond 40% saturation, the graph begins to plateau, reaching a critical saturation point at approximately 70%, where resistivity becomes relatively constant. This behavior aligns with the findings of Mustofa et al. (2021) and Knight (1991), who identified the critical

saturation point as occurring between 50% and 70%.

Among the three sample categories (A, B, and C), sample C exhibited the lowest resistivity before reaching the critical saturation point. This result may be attributed to differences in pore structure and physical properties such as permeability. Samples A, B, and C have varying permeability levels, with sample A showing the highest permeability and sample C the lowest (Mustofa et al., 2021). Additionally, compaction under wet conditions may reduce resistivity, as suggested by Abu-Hassanein et al. (1996). The smaller grain sizes in sample C make it more susceptible to compaction. reducina pore space consequently lowering resistivity.

Partially Saturated

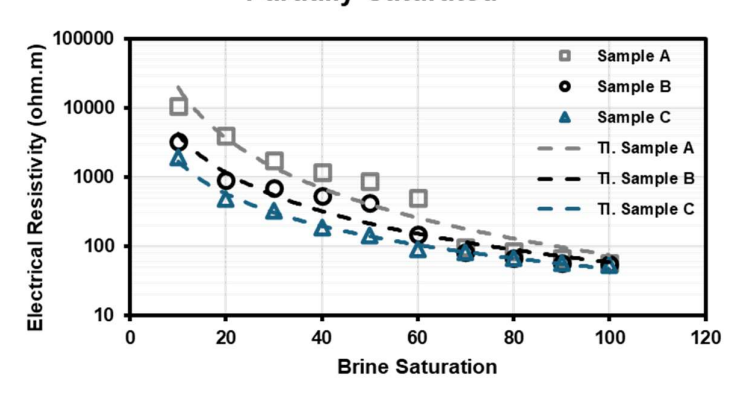


Figure 4. Relationship between measured resistivity and brine saturation for: (a) dry conditions and (b) partially saturated conditions.

3.3 Microstructure of Sample

Scanning results for samples A (mesh 20), B (mesh 40), and C (mesh 60) are shown in Figure 5. The images demonstrate that grain size decreases progressively from sample A to sample C.

Microstructural data, including porosity, pore structure, and grain size distribution, were also derived from these scans.

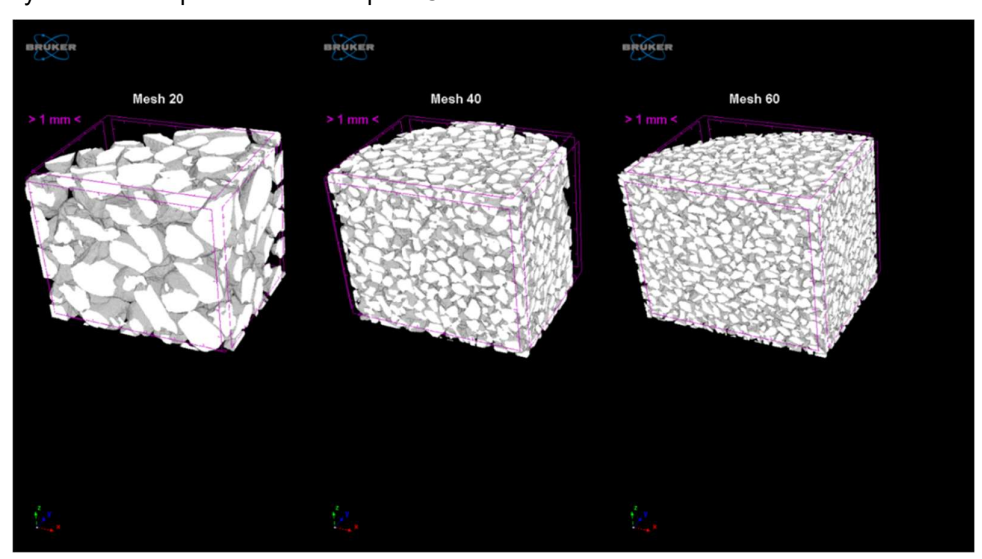


Figure 5. Digital reconstructions of (a) sample A (mesh 20), (b) sample B (mesh 40), and (c) sample C (mesh 60).

Porosity data from the scans are presented in Figure 6, comparing 2D (total and open) and 3D porosity. For sample A, open porosity ranged from 17% to 41% (average: 36.11%), total porosity ranged from 31% to 43% (average: 40.36%), and 3D porosity was 40.81%. For sample B, open porosity ranged from 4% to 38% (average: 25.39%), total porosity ranged from 37% to 44%

(average: 40.84%), and 3D porosity was 41.49%. For sample C, open porosity ranged from 0.7% to 18% (average: 3.89%), total porosity ranged from 27% to 34% (average: 33.86%), and 3D porosity was 34.46%. These results are in accordance with the results of porosity measurements as presented in the previous section.

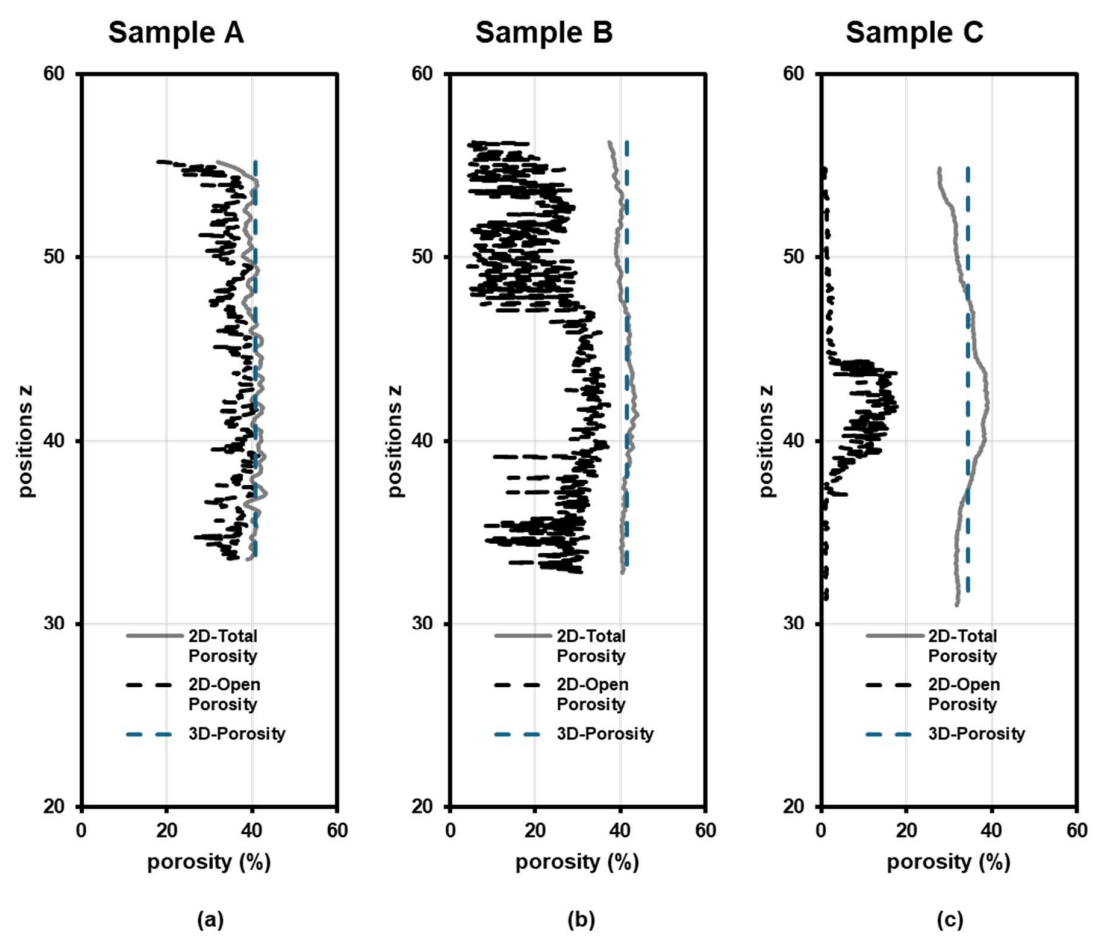


Figure 6. Distribution of 2D and 3D porosity based on digital images for: (a) sample A, (b) sample B, and (c) sample C.

Pore and grain size distributions were also analyzed using digital rock physics, as shown in Figure 7. Across all three samples, the peak of the pore size distribution was consistently smaller (shifted leftward) than the peak of the grain size distribution. Maximum grain sizes were 1.603 mm for sample A and 0.962 mm for samples B and C.

In contrast, maximum pore sizes were 1.318 mm, 0.891 mm, and 0.534 mm for samples A, B, and C, respectively. The characteristics of the pore and grains size distribution will affect the physical properties of the rock itself (Verwer et al., 2011; Torskaya et al., 2014).

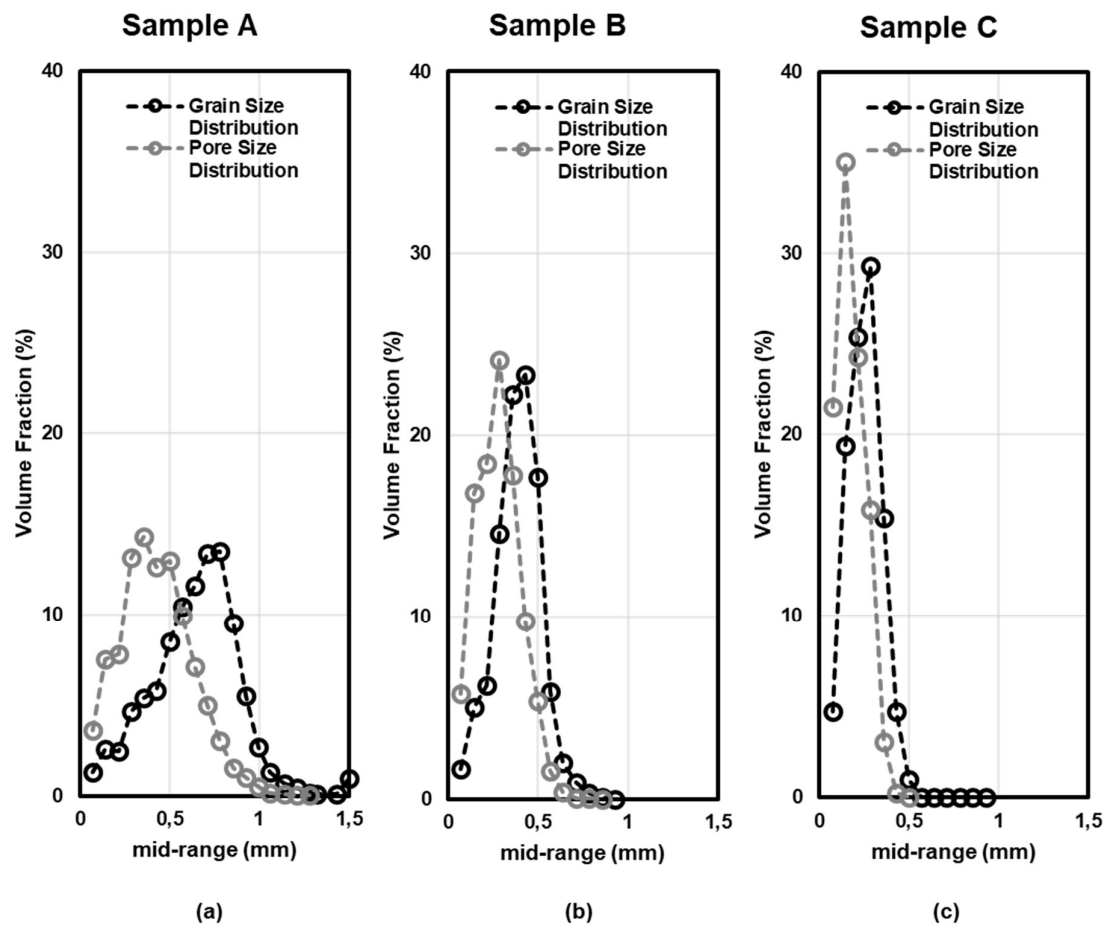
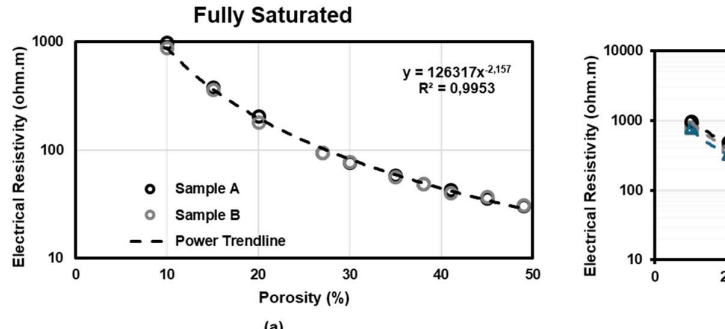


Figure 7. Pore and grain size distributions based on digital images for: (a) sample A, (b) sample B, and (c) sample C..

3.4 Calculated Resisitivity

Electrical resistivity calculations were performed under two conditions: fully saturated (samples A and B) and partially saturated (samples A, B, and C), as illustrated in Figure 8. Under fully saturated conditions, the relationship between porosity and resistivity for samples A and B exhibited similar trends. The power trendline produced R^2 values close to 1, with a slope (m) of 2.157. This result suggests that, based on Digital Rock Physics (DRP) analysis, the porosity-resistivity relationship is not significantly affected by grain size.

In partially saturated conditions, resistivity values decreased consistently with increasing fluid saturation across all samples, particularly within the 70%-100% saturation range. This finding aligns with previous studies, indicating that grain size variations have minimal impact on resistivity-saturation relationships at high saturation levels (Mustofa et al., 2022). However, at low saturation levels, sample C consistently displayed the lowest resistivity values compared to samples A and B.



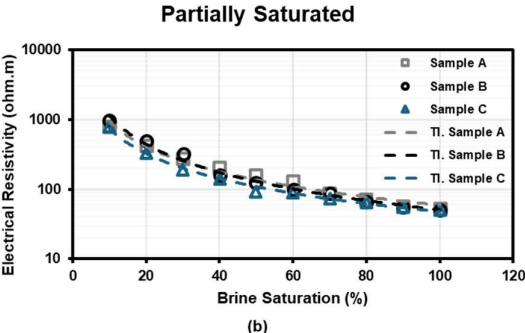
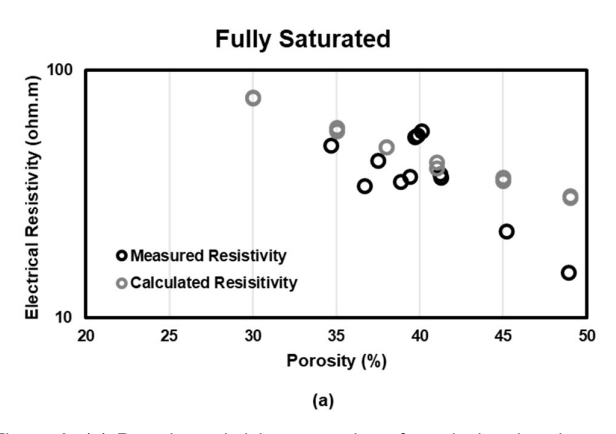


Figure 8. Electrical resistivity calculations for: (a) fully saturated conditions and (b) partially saturated conditions.

3.5 Microstructure vs Calculation

A comparison of measured and calculated resistivity was conducted for both fully and partially saturated conditions. For fully saturated conditions, the relationship between porosity and resistivity is shown in Figure 9. While minor discrepancies were observed at porosities above 45%, the overall

agreement between calculated and measured results was strong (see Figure 9a). This relationship can expressed be as $\rho_{cal} =$ R^2 $0,673\rho_{meas} + 19,757$ with value approximately 0.812, indicating a good correlation. (see Figure 9b).



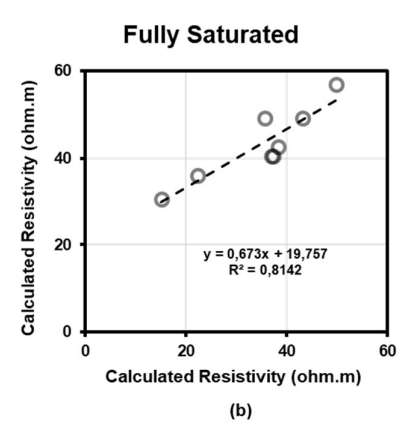


Figure 9. (a) Porosity-resistivity comparison for calculated and measured values, and (b) linear relationship between calculated and measured resistivity.

For partially saturated conditions, the resistivity-saturation relationship is illustrated in Figure 10. For sample A, calculated resistivity underestimated the measured values at saturation levels below 70% but showed good alignment above this threshold (see Figure 10. a and 10.b). For sample B, overall agreement was strong, with only minor

discrepancies observed around the 40%-50% saturation range (see Figure 10.c and 10.d). Sample C demonstrated the best alignment, with calculated and measured resistivity values exhibiting a very strong correlation with $R^2 = 0.9839$ (see Figure 10.e and 10.f).

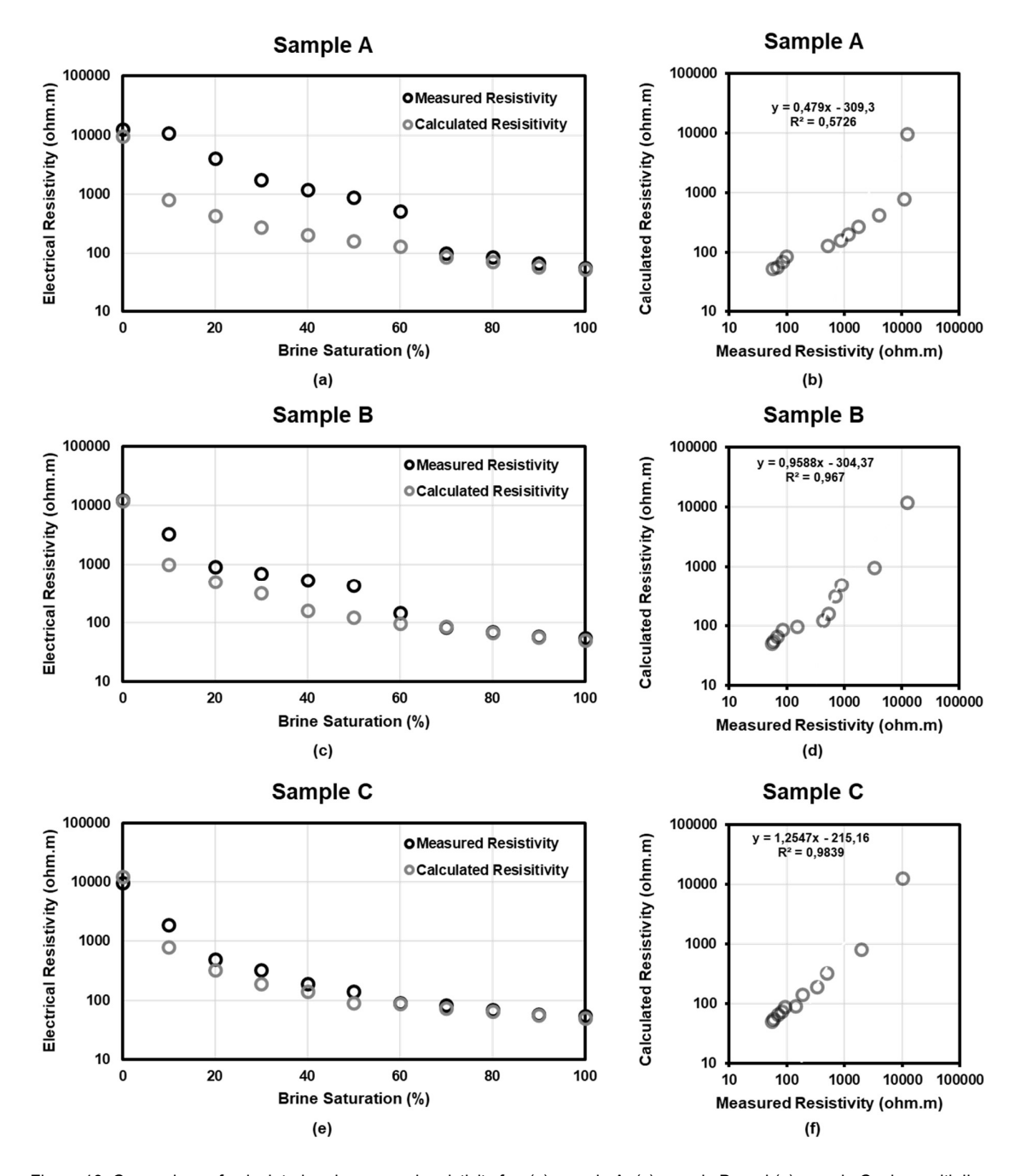


Figure 10. Comparison of calculated and measured resistivity for: (a) sample A, (c) sample B, and (e) sample C, along with linear relationships for (b) sample A, (d) sample B, and (f) sample C.

Archie parameters, including the cementation exponent (m) for fully saturated conditions and the saturation exponent (n) for partially saturated

conditions, are summarized from the measurements and calculations in Table 2.

Table 2. Archie parameters based on measured and calculated results.

Fully Saturated				
	а	т	R^2	
Measurement	10^7	3,418	0,8654	
Calculation	1,2x10^5	2,157	0,9953	

Partially Saturated				
	а	n	R^2	
Sample A				
Measurement	5x10^6	2,422	0,9639	
Calculation	1,4x10^4	1,201	0,9808	
Sample B				
Measurement	3x10^5	1,850	0,9836	
Calculation	2,5x10^4	1,348	0,9816	
Sample C				
Measurement	6x10^4	1,548	0,9925	
Calculation	1,1x10^4	1,196	0,998	

4. Conclusion

The electrical properties of unconsolidated Ngrayong sandstone samples were analyzed using both laboratory measurements and numerical simulations. The porosity-resistivity relationship produced a cementation exponent (m) ranging from 2.1 to 3.4, while the resistivity-saturation relationship yielded a saturation exponent (n) of 1.2 to 2.4. At low saturation levels (<70%), grain size significantly influenced resistivity, with smaller grains resulting in lower resistivity values. However, at high and full saturation levels, grain size had minimal impact on resistivity. The correlation between measured and calculated results was generally strong ($R^2 > 0.812$), except for sample A, which had the largest grain size. Numerical simulations effectively replicated the physical phenomena observed in laboratory measurements, though for sample A, the saturation model may require further refinement.

This study provides a more detailed characterization of how grain size influences the electrical properties of Ngrayong sandstone, offering a refined understanding of its behavior at varying saturation levels. This research integrates both laboratory and numerical approaches to validate the observed trends, enhancing its reliability. These findings contribute valuable

insights for hydrocarbon reservoir analysis and applied geophysics, particularly in improving resistivity-based formation evaluation models.

References

Andrä, H., Combaret, N., Dvorkin, J., Glatt, E., Han, J., Kabel, M., Keehm, Y., Krzikalla, F., Lee, M., Madonna, C., Marsh, M., Mukerji, T., Saenger, E. H., Sain, R., Saxena, N., Ricker, S., Wiegmann, A., & Zhan, X. (2013a). Digital rock physics benchmarks-Part I: Imaging and segmentation. Computers and Geosciences, 50,
25–32.

https://doi.org/10.1016/j.cageo.2012.09.005

Andrä, H., Combaret, N., Dvorkin, J., Glatt, E., Han, J., Kabel, M., Keehm, Y., Krzikalla, F., Lee, M., Madonna, C., Marsh, M., Mukerji, T., Saenger, E. H., Sain, R., Saxena, N., Ricker, S., Wiegmann, A., & Zhan, X. (2013b). Digital rock physics benchmarks-part II: Computing effective properties. Computers and 50. Geosciences. 33-43. https://doi.org/10.1016/j.cageo.2012.09.008

Abu-Hassanein, Z. S., Benson, C. H., & Blotz, L. R. (1996). Electrical resistivity of compacted clays. Journal of Geotechnical Engineering, 122(5), 397–406.

Andra, H., Combaret, N., Dvorkin, J., Glatt, E., Han, J., Kabel, M., . . . Zhan, X. (2013). Digital rock

- physics benchmarks—Part I: Imaging and segmentation. Computers & Geosciences, 50, 25-32.
- Archie, G. E. (1942). The electrical resistivity logs as an aid in determining some reservoir characteristics. Transactions of AIME, 146, 54–62.
- Blunt, M. J., Bijeljic, B., Dong, H., Gharbi, O., Iglauer, S., Mostaghimi, P., Paluszny, A., Pentland, C. (2013). Advances in water resources pore-scale imaging and modelling. Advances in Water Resources, 51, 197–216. https://doi.org/10.1016/j.advwatres.2012.03.00
- Dhamayanti, E., Raharjanti, N., & Hartati, I. (2016).

 Dinamika sedimentasi singkapan Formasi
 Ngrayong dengan analogi lingkungan
 pengendapan modern, studi kasus singkapan
 Polaman dan Braholo dengan analogi pesisir
 pantai Utara Jawa.
- Glover, P. W. J. (2017). A new theoretical interpretation of Archie's saturation exponent. Solid Earth, 8(4), 805–816. https://doi.org/10.5194/se-8-805-2017
- Knight, R. (1991). Hysteresis in the electrical resistivity of partially saturated sandstones. Geophysics, 56(12), 2139–2147. https://doi.org/10.1190/1.1443028
- Kadar, D., & Sudijono. (1993). Systematic geological map, Indonesia, Quadrangle Rembang 1509-1 and 6 Scale 1:100,000: Geological Research and Development Centre.
- Latief, F. D. E., Fauzi, U., Irayani, Z., & Dougherty, G. (2017). The effect of X-ray micro computed tomography image resolution on flow properties of porous rocks. Journal of Microscopy, 266(1), 69–88. https://doi.org/10.1111/jmi.12521
- Müller-Huber, E., Schön, J., & Börner, F. (2015). The effect of a variable pore radius on formation resistivity factor. Journal of Applied Geophysics, 116, 173–179. https://doi.org/10.1016/j.jappgeo.2015.03.011

- Mustofa, M. B., Fauzi, U., Warsa, W., & Latief, F.
 D. E. (2022). Experimental and modeling of electrical resistivity changes due to microspatial distribution of fluid for unconsolidated sand. Journal of Petroleum Science and Engineering, 208, 109472. https://doi.org/10.1016/j.petrol.2021.109472
- Mustofa, M. B., Fauzi, U., Warsa, W., Latief, F. D. E., et al. (2021). The effect of brine spatial distribution on electrical resistivity during imbibition processes in unconsolidated sands. Journal of Applied Geophysics. https://doi.org/10.1016/j.jappgeo.2021.104441
- Nababan, B., Zanetta, E., Novia, N., & Handoyo, H. (2019). Estimasi nilai porositas dan permeabilitas dengan pendekatan digital rock physics (DRP) pada sampel batupasir Formasi Ngrayong, Cekungan Jawa Timur bagian utara. Jurnal Geofisika Eksplorasi, 5(3), 193–203. https://doi.org/10.23960/jge.v5i3.34
- Pringgoprawiro, H. (1983). Biostratigrafi dan paleogeografi Cekungan Jawa Timur Utara: Suatu pendekatan baru. Institut Teknologi Bandung.
- Sezgin, E. E., & Akın, M. (2013). Sensitivity of Archie's parameters (m and n) in prediction of reservoir fluid saturation and porosity. Journal of Petroleum Science and Engineering, 107, 63–71.
 - https://doi.org/10.1016/j.petrol.2013.04.009
- Torskaya, T., Shabro, V., Torres-Verdín, C., Salazar-Tio, R., & Revil, A. (2014). Grain shape effects on permeability, formation factor, and capillary pressure from pore-scale modeling. Transport in Porous Media, 102(1), 71–90. https://doi.org/10.1007/s11242-013-0262-7
- Tariq, M. R., & Kazi, M. R. (2017). Optimization of Archie's Law parameters for estimating porosity and fluid saturation in carbonate reservoirs. Journal of Petroleum Technology, 69(12), 1241–1255. https://doi.org/10.2118/1234567-JPT

Vozar, J., & Gurevich, B. (2014). Sensitivity of electrical resistivity tomography to geological structures: A numerical study. Geophysics, 79(2), B35–B47. https://doi.org/10.1190/geo2013-0456.1

Zhou, Y., & Zhang, L. (2020). Use of geoelectric resistivity method for geological structure

delineation and groundwater exploration in fractured rocks. Journal of Hydrology and Earth System Sciences, 24(6), 2041–2055. https://doi.org/10.5194/hess-24-2041-2020